The definitive publisher version is available online at
https://doi.org/10.1016/j.jenvman.2022.115497

Adsorption and desorption behavior of arsenite and arsenate at river sediment-water interface

Kien Thanh Nguyen[a], Amir Hossein Navidpour[a], Mohammad Boshir Ahmed[b], Amin Mojiri[c], Yuhan Huang[a], John L. Zhou[a,*]

[a] Centre for Green Technology, School of Civil and Environmental Engineering, University of Technology Sydney, 15 Broadway, NSW 2007, Australia

[b] School of Material Science and Engineering, Gwangju Institute of Science and Technology, Gwangju, 61005, Republic of Korea

[c] Department of Civil and Environmental Engineering, Graduate School of Advanced Science and Engineering, Hiroshima University, 1-4-1 Kagamiyama, Higashihiroshima, 739-8527, Hiroshima, Japan

Corresponding author:

Prof. John L Zhou, Email: junliang.zhou@uts.edu.au

Abstract

The adsorption of inorganic arsenic (As) plays an important role in the mobility and transport of As in the river environment. In this work, the adsorption and desorption of arsenite [As(III)] and arsenate [As(V)] on river sediment were conducted under different pH, initial As concentrations, river water and sediment composition to assess As adsorption behavior and mechanism. Both adsorption kinetics and equilibrium results showed higher adsorption capacity of sediment for As(V) than As(III). Adsorption of As(III) and As(V) on river sediment was favored in acidic to neutral conditions and on finer sediment particles, while sediment organic matter marginally reduced adsorption capacity. In addition, higher adsorption affinity of As(III) and As(V) in river sediment was observed in deionised water than in river water. For the release process, the desorption of both As(III) and As(V) followed nonlinear kinetic models well, showing higher amount of As(III) release from sediment than As(V). Adsorption isotherm was well described by both Langmuir and Freundlich models, demonstrating higher maximum adsorption capacity of As(V) at 298.7 mg/kg than As(III) at 263.3 mg/kg in deionised water, and higher maximum adsorption capacity of As(III) of 234.3 mg/kg than As(V) of 206.2 mg/kg in river water. The XRD showed the changes in the peaks of mineral groups of sediment whilst FTIR results revealed the changes related to surface functional groups before and after adsorption, indicating that Fe–O/Fe–OH, Si(Al)–O, hydroxyl and carboxyl functional groups were predominantly involved in As(III) and As(V) adsorption on sediment surface. XPS analysis evidenced the transformation between these As species in river sediment after adsorption, whilst SEM-EDS revealed higher amount of As(V) in river sediment than As(III) due to the lower signal of Al.

Keywords: Arsenic adsorption; Adsorption kinetics; Adsorption isotherm; River sediment; Sediment functional groups

1. Introduction

Arsenic (As) is a highly toxic element, and its contamination in soils, sediments, surface water and groundwater has been widely monitored due to significant threat to plants, animals and human health (Dousova et al., 2012). Natural and anthropogenic processes cause an increasing amount of As into sediments and water environment (Goldberg and Suarez, 2013; Zhang and Selim, 2005). Anthropogenic activities are the main sources of As contamination in soils and sediments (Dousova et al., 2012), among which mining is the second largest source contributing to highly contaminated As levels in the environment. As exists in the natural environments in two main soluble forms, i.e. arsenate [As(III)] and arsenite [As(V)] (Arco-Lázaro et al., 2016). As(III) is predominant under reducing conditions, while As(V) is prevalent under oxidizing conditions (Dousova et al., 2012). High abundance and toxicity of inorganic arsenics have received major attention from scientists to examine As transportation behavior (Wang et al., 2018).

Adsorption is a key process regulating As transport in the aquatic environment. Adsorption kinetics, mechanisms and controlling parameters such as pH, phosphate, temperature, sediment organic matter (SOM), texture, and clay minerals have been studied (Arco-Lázaro et al., 2016; Dousova et al., 2012) for a better understanding of As sorption mechanisms. The effect of pH on As adsorbed on sediments has been investigated by Ma et al. (2015), who indicated that the amount of As(III) and As(V) adsorbed on sediment increased when pH decreased from 9 to 5. Adsorption of As is highly dependent on sediment properties (Xie et al., 2018) and environmental conditions. SOM has shown negative impacts on As adsorption, whilst small particle size of sediment enhances As adsorption on soils (Nguyen et al., 2021). Wang and Mulligan (2006) suggested that humic and fulvic acids had a high affinity for adsorption to the metal (hydro)oxide surface, resulting in competition with As(III) and As(V) for adsorption on the sediment surfaces. However, the authors explained that As(III) and As(V) ions may be strongly bound with the formation of SOM-metal complexes through metal-bridging

mechanisms, through which these As species form aqueous complexes with humic and fulvic acids. In addition, SOM could control the release of As(V) from solid phase regardless of the adsorption mechanism (Grafe et al., 2001). Varsányi and Kovács (2006) showed a strong correlation between As and sediment organic carbon (SOC) at low SOC (0.04%) and high Fe (4.91 g/kg) concentrations, but no such correlation was observed at high SOC (0.775% and 0.810%) and low Fe (0.09% and 0.29%) concentrations. Therefore, the effect of SOM on As(III) and As(V) adsorption on sediment is still not entirely clear. Regarding the grain size of sediment, Dias et al. (2009) considered sediment textural fractions as the most important parameter influencing As(V) adsorption on sediments. Smith et al. (2006) and Xie et al. (2018) found that the adsorption of total and inorganic As species [As(III) and As(V)] on sediments increased with decreasing particle size, with sand < silt < clay. For instance, the adsorption capacity of As(III) on sediments increased from 1.57 mmol/kg to 2.62 mmol/kg for sandy and clay types, and from 2.81 mmol/kg to 5.13 mmol/kg for As(V) (Xie et al., 2018). Hence, the adsorption of As(III) and As(V) on different sediments has been studied; however, the contribution of different sediment size fractions still needed further investigation.

The adsorption and desorption rates of As on sediments were studied by Xie et al. (2018). They found that the adsorption of As(III) and As(V) occurred rapidly during the first two days, slowed down in the next five days, and then became relatively stable until 28 days. Similarly, the release of As from sediment into water rapidly decreased after seven days, followed by a slow rate. Furthermore, the desorption rate of As(III) reached a maximum of 60% which was higher than that of As(V) at 40% (Xie et al., 2018). Overall, As adsorption from water and its controlling factors have been widely investigated. Recent studies on the interactions between As species and adsorbent surfaces indicated that As(V) mainly interacted with COOH, O-H and Fe-O functional groups of soils (Rawat et al., 2022), while As(III) adsorption on microplastics mainly occurred via hydrogen bond of carboxyl group (Dong et al., 2019; 2020). Up to now, the study on As desorption has been limited to soils, though this desorption process and

consequent As migration to the environment are of great importance (Feng et al., 2013).

In river sediments, As predominantly exists as arsenite [As(III)] in the anoxic zone, and as arsenate [As(V)] in the oxic surface layer (Dousova et al., 2012). The average abundance of As in the crustal earth is 1.5 mg/kg, ranging from <1 to 15 mg/kg in alluvial sands, glacial till, lake sediments and soils (Plant et al., 2005). According to Hettiarachchi et al. (2017), only inorganic species were present in mangrove sediments located in southeast New South Wales, Australia. As contamination in river sediment can cause tremendous harm to living organisms, even at low concentrations (De Jonge et al., 2012; Tang et al., 2017). Adsorption and desorption are key geochemical processes in river environments regulating As transport and fate in river systems. River sediments play a vital role in removing As from contaminated water, and can also act as a secondary pollution source releasing As into the surface water and groundwater (Chen et al., 2017; Lou et al., 2017).

The adsorption behavior of As on sediments has been reported (Dousova et al., 2012; Goldberg and Suarez, 2013; Ma et al., 2015); however, the contribution of sediment physicochemical characteristics to As adsorption or retention is still not clear. Therefore, the interactions between As species and river sediment were investigated in this study in order to develop better understanding and sustainable management strategies for arsenic contaminated sediments. Therefore, this paper aims to examine the adsorption kinetics, adsorption isotherms and adsorption mechanisms of As(III) and As(V) on river sediment under different conditions.

2. Materials and methods

2.1. Chemical standards

Multi-element standard solution 4 for ICP (40 mg/L of As) was supplied by Sigma-Aldrich Pty Ltd, Australia. The solution was diluted by Milli-Q water with a resistivity of 18 MΩ. All chemicals were of analytical grade. Sodium arsenate dibasic heptahydrate ($Na_2HAsO_4{\cdot}7H_2O$) and sodium arsenite ($NaAsO_2$), purchased from Sigma-Aldrich Pty Ltd, were dissolved with

Milli-Q water to obtain As(III) and As(V) stock solution (100 mg/L). The phosphoric acid (H_3PO_4, 85% w/w) and hydroxylamine hydrochloride ($NH_2OH{\cdot}HCl$, 99% purity) were also obtained from Sigma-Aldrich Pty Ltd. Then, the solutions of 1.0 M phosphoric acid and 0.2 M hydroxylamine hydrochloride were prepared by diluting their original standard solutions with Milli-Q water. All plasticware and glassware were soaked in 2% (v/v) HNO_3, followed by repeated rinsing with deionized water, then were dried before use.

2.2. Field sampling

Bargo River, New South Wales, Australia receives treated wastewater due to coal mining activities from the Teatree Hallow (Supplementary Materials **Fig. S1**). Bargo River water was not determined as polluted, whilst river sediment was reported as unpolluted to moderately polluted with heavy metals due to mining activity (Ali et al., 2018). Therefore, Bargo River sediment was chosen as natural adsorbent for As sorption and desorption experiments. The Teatree Hallow river receives treated wastewater from underground coal mining activity and discharges to Bargo River at the point (34°14'35.1"S; 150°35'16.7"E). Samples were collected at the bottom of the Bargo River, about 3.5 km from the junction point with the Teatree Hollow. Clean 5-L plastic containers were rinsed three times by river water, then filled up by river water, sealed before transporting to the laboratory and kept at room temperature for adsorption/desorption experiments. In addition, clean 200-mL plastic bottles were rinsed three times before filling up by river water, then sealed by caps. The bottles were stored in a cool box at 4 °C when transferring to the laboratory for analysing the concentrations of As compounds. The sediment samples were packed in sealed polyethylene bags, then stored in a cool box at 4 °C when transferred to the laboratory. The sediment samples were dried in an oven at 105 °C for 24 h, then passed through 2-mm sieve before further analysis.

150 *2.3. River water and sediment characterization*

151 River water was analysed in triplicate to determine the concentrations of metals (As, Fe, Al, Ni,
152 Cu and Pb) by ICP-MS (Agilent 7900) and total organic carbon (TOC) content by multi N/C
153 3100 TOC analyzer by Analytik Jena, Germany. The content of SOM was determined by the
154 loss-on-ignition (LOI) method, by sediment combustion at 550 ^{o}C, according to Hoogsteen et
155 al. (2018). The combusted sediment was named as river sediment without organic matter (RS-
156 NOM). In addition, the river sediment was fractionated by sieving through a series of sieves to
157 obtain gravel and coarse sand (fraction S_1, 300-2000 μm), medium sand (fraction S_2, 150-300
158 μm), fine sand (fraction S_3, 75-150 μm), and clay-silt (fraction S_4, < 75 μm). The specific
159 surface area (SSA) of the dried sediment and different sizes were measured by a Quantachrome
160 surface area analyzer using the Brunauer–Emmett–Teller (BET) method.

161 The extraction of As from sediment was conducted by following a method by Ellwood and
162 Maher (2003). Briefly, sediment (1.0 g) was accurately weighed into a 50-mL Teflon centrifuge
163 tube, to which 5 mL of phosphoric acid (1.0 M) and 5 mL of hydroxylamine hydrochloride (0.2
164 M) were added. The samples were shaken on a horizontal shaker at 120 rpm for 1 h before
165 centrifugation. Aliquots of the supernatant were removed and filtered through 0.45 μm filters
166 before As analysis. According to Ellwood and Maher (2003), around 90% of extractable As
167 was obtained by using this method.

168

169 *2.4. Batch experiments for adsorption and desorption*

170 The adsorption of As(III)/As(V) was assessed for different sediments including dried river sediment
171 (RS), RS-NOM, and four particle size fractions including S_1, S_2, S_3 and S_4. The stock solution of
172 100 mg/L of As(III)/As(V) was diluted by Milli-Q water to obtain 0.1-10 mg/L solution. The
173 adsorption kinetics experiments were conducted by mixing 200-mL of As(III) or As(V) (0.1-
174 10.0 mg/L) with 2.0 g of sediment, which were mixed on a shaker at 120 rpm. During adsorption,
175 2 mL suspension samples were taken at regular intervals (3, 6, 12, 24, 72, 120, 168 h), filtered by

a 0.45 μm membrane filter, and analyzed for total As by ICP-MS (Agilent 7900). The adsorption of As(III) or As(V) was evaluated by monitoring the decrease of arsenic concentration in solution.

For the adsorption isotherm experiments, a series of As(III)/As(V) solutions with different initial concentrations (0.1, 0.25, 0.5, 1.0, 2.0, 5.0 and 8.0 mg/L) were prepared by diluting the stock solution (100 mg/L) with Milli-Q water. Then, sediment (2.0 g) was mixed with 200 mL of As solution in 500 mL beakers, which were shaken on a horizontal shaker at 120 rpm for 7 days. The pH of feeding solutions was adjusted to 4 ± 0.2 and 10 ± 0.2 by diluted nitric acid (0.1 M HNO_3) and sodium hydroxide (0.1 M NaOH) at the initial time of adsorption

The desorption experiments were conducted immediately after the completion of adsorption process of As(III) and As(V) on RS. The supernatant was removed and replaced by 200 mL Milli-Q water, the vials resealed and shaken at 120 rpm for 48 h. Aliquot (3 mL) was sampled from the supernatant at different reaction times (3, 6, 12, 24, 72, 120 and 168 h), then filtered and analyzed for total As concentration using ICP-MS (Agilent 7900). The fractions of As(III) and As(V) desorbed from RS were calculated from the mass balance results based on the changes in As(III) and As(V) concentrations in solution before and after desorption.

2.5. Sediment surface functional groups and minerals

The sediment samples were ground to fine power before analysis. The FTIR spectra (500-4000 cm^{-1}) of different sediments including RS, RS-NOM and sediment fractions before and after adsorption of As(III) and As(V) were analyzed by using Shimadzu MIRacle 10 (Japan) in order to investigate sediment surface sorption mechanisms. Additionally, sediments were analyzed by the X-ray diffraction (XRD) on a Bruker D8 Discover XRD, to examine how crystalline materials in sediments were involved in As interactions. River sediment surface before and after adsorption was examined by scanning electron microscopy (SEM) and energy dispersive X-ray spectroscopy (EDS) method by Oxford Aztec instrument, while X-Ray Photoelectron

Spectroscopy (XPS) from ESCALAB™ QXi X-ray Photoelectron Spectrometer (XPS) Microprobe, Thermo Scientific, UK was used to examine the surface of RS particles.

2.6. Kinetic and equilibrium sorption studies

Arsenic concentrations retained in the adsorbent phase (mg/kg) were calculated by following formula:

$$q_t = \frac{(C_o - C_t)V}{m} \quad (1)$$

$$q_e = \frac{(C_o - C_e)V}{m} \quad (2)$$

where q_t (mg/kg) and C_t (mg/L) are the concentrations of As(III) or As(V) in sediment and solution at time t; q_e (mg/kg) and C_e (mg/L) are the concentrations of As(III) or As(V) in sediment and solution at the equilibrium time; C_o (mg/L) is As(III) or As(V) concentration at the initial time; V (mL) is volume of solution; m is the weight of adsorbent (g).

The pseudo first-order (PFO) and pseudo second-order (PSO) equations have been widely applied to assess the adsorption of As on soils, sediments and MPs (Dong et al., 2020, 2019; Gedik et al., 2016; Guo et al., 2007; Kumar et al., 2016; Kundu and Gupta, 2006; Luo et al., 2019; Ma et al., 2015; Rawat et al., 2021). The PFO model can well describe the initial adsorption stage (Ho and McKay, 1999; Ma et al., 2015), while the PSO model is better for describing the physical or chemical adsorption at a site (Kumar et al., 2016) or the whole adsorption process (Ma et al., 2015).

The adsorption experimental data was analysed by PFO and PSO kinetic models using non-linear regression equations (Alkurdi et al., 2021; Ma et al., 2015). The linear forms of PFO and PSO kinetic models are straightforward for application, however, the erroneous values of calculating kinetic parameters were the drawbacks (Azizian, 2004). In contrast, the non-linear forms provided better results in comparison to linear regression analysis (Rawat et al., 2021). Thus, the non-linear forms of PFO and PSO models for the adsorption kinetics are used in this study (Ma et al., 2015):

$$q_t = q_e(1 - e^{-k_1 t}) \quad (3)$$

$$q_t = \frac{q_e^2 k_2 t}{1+q_e k_2 t} \quad (4)$$

For the desorption process, the PFO and PSO models are described as below (Tseng et al., 2009):

$$q_t = q_e + (q_o - q_e)\exp(-k_1 t) \quad (5)$$

$$q_t = q_e + \frac{q_e - q_o}{k_2(q_e - q_o)t - 1} \quad (6)$$

where q_o is the amount (mg/kg) of As(III) or As(V) at the initial time of desorption.

The adsorption phenomenon at the interface between solid and liquid phases is widely interpreted by the Langmuir and Freundlich isotherms (Tseng et al., 2009). The Langmuir isotherm model (equation 7) is used to describe the monolayer adsorption, which is expressed as below (Rawat et al., 2022):

$$q_e = \frac{K_L q_m C_e}{1+K_L C_e} \quad (7)$$

where K_L and q_m represent the bonding energy constant (mg/L) and the maximum adsorption capacity (mg/kg), respectively.

Additionally, the equilibrium parameter (R_L) was used to explain the essentiality of Langmuir adsorption isotherms by equation 8 (Rawat et al., 2022):

$$R_L = \frac{1}{1+K_L C_e} \quad (8)$$

The values of $R_L > 1$, $0 < R_L < 1$, $R_L = 1$, and $R_L = 0$ indicate unfavorable, favorable, linear and irreversible adsorption of As(III) and As(V) on the surface of sediment particles, respectively (Rawat et al., 2022).

The Freundlich sorption model (equation 9) is an empirical adsorption equation indicating that adsorption sites on the surface of adsorbent possess different adsorption energies, which can be expressed as (Wang et al., 2018):

$$q_e = K_F \times C_e^{1/n} \quad (9)$$

where K_F is the Freundlich constant or capacity factor (mg/kg-(L/mg)^n), while $1/n$ is the Freundlich exponent (Rawat et al., 2022).

A three-parameter isotherm model, Sips (equation 10) is formed by the combination from Langmuir and Freundlich expressions (Alkurdi et al., 2021). This model reduces to the Freundlich model at the low adsorbate concentrations or to the Langmuir model while the adsorbate concentrations are high (Foo and Hameed, 2010).

$$q_e = \frac{q_m K_s C_e n_s}{(1+K_s C_e n_s)} \quad (10)$$

where K_s is the Sips constant related to the energy of adsorption process, and n_s is the exponential factor of the isotherm.

The sediment-solution partition coefficient (K_p) was used to describe the interactions of heavy metals at the interface between water and sediment phases (Fang et al., 2021). K_p provides the information of combined effect of adsorption and desorption processes of heavy metals (Nematollahi et al., 2021). In addition, it was also used for modelling metal transfer in various catchment scales or hydraulic systems such as rivers or lakes. Garneau et al. (2015) used K_p as a sub-model of adsorption and desorption processes to simulate As transport in the Garonne River, France. In this study, the K_p of As at sediment-water interface was calculated by equation 11 (Zhou and Broodbank, 2014):

$$K_p = \frac{q_e}{C_e} \text{ (L/kg)} \quad (11)$$

3. Results and discussion

3.1. Characteristics of river water and sediment

The total As content and other physicochemical characteristics of the Bargo river water were analysed, in comparison with results reported for Teatree Hallow in September 2021 receiving treated wastewater due to coal mining activities by SIMEC group in New South Wales, Australia (**Table 1**). The metals concentrations in Bargo River water were lower than its upstream, Teatree Hallow, except the Al concentration, due to the dilution, sorption and sedimentation processes. All water quality values in Bargo River and Teatree Hallow were below the standard of Australia freshwater (AWQG, 1992), except concentrations of Ba and Zn

in Teatree Hallow. Hence, water quality in Bargo River and its tributary was slightly polluted in some cases.

Table 1. River water characteristics from Bargo River, NSW, Australia and its tributary.

	Bargo river (this study)	**Teatree Hallow**	**AWQG[a]**	**Unit**
Al	35.69 ± 4.95	30	100	µg/L
As	12.93 ± 0.29	56	50	µg/L
Ba	307.72 ± 21.66	1590	1000	µg/L
Cr (total)	8.32 ± 0.01		10	µg/L
Cu	2.02 ± 0.56	1	2-5	µg/L
Fe (total)	110.77 ± 13.71		1000	µg/L
Mn	2.93 ± 0.25		100	µg/L
Ni	11.09 ± 0.22	30	15-150	µg/L
Pb	17.24 ± 0		1-5	µg/L
Zn	48.99 ± 0.53	71	5-50	µg/L
Electrical Conductivity	473 ± 10	1930		µg/L
Turbidity	223 ± 5			
TOC	30.20 ± 0.26			mg/L
References	This study	SIMEC (2021)	SIMEC (2021)	

a. Australian Water Quality Guidelines for Freshwater.

The As concentration and important physicochemical characteristics of the river sediment compared to other sediments collected in New South Wales, Australia are summarized in **Table 2**. The metal concentrations in this study were lower than those reported by Fleming et al. (2021), who collected the samples closer to coal mining. **Table 2** indicated that sediment quality in New South Wales, Australia related to heavy metals is influenced by coal mining activities, although the concentrations of As and other heavy metals (Cd, Cr, Ni, Pb and Zn) are below the default guideline values (DGV) for sediment in Australia. Thus, the selected sediment in this study is not contaminated above background value. In addition, these heavy metal

293 concentrations were lower than those of other sediments collected from several ports in New
294 South Wales (Jahan and Strezov, 2018). It is suggested that the treated wastewater from mining
295 activities in the upstream area enhanced metal loading in polluted sediments downstream. The
296 As concentration (0.16 mg/kg) in this sediment was remarkably lower than average
297 concentrations of As (32.0 mg/kg) in three mangrove surface sediments collected at Candalagen
298 Creek, Batemans Bay and Sussex inlet in southeast New South Wales, Australia (Hettiarachchi
299 et al., 2017). The SSA of the river sediment (4.6 m^2/g) was similar to sediments collected from
300 the Elbe River basin in the Czech Republic (7.3 m^2/g and 3.5 m^2/g) although the SOC content
301 in this study was lower than any sediments investigated by Dousova et al. (2012).

302 **Table 2.** The composition of Bargo River sediment (in triplicate), in comparison to other sediments in New South Wales, Australia

	SSA (m^2/g)	SOM (%)	Al (mg/kg)	Fe (mg/kg)	As (mg/kg)	Cr (mg/kg)	Ni (mg/kg)	Zn (mg/kg)	Cd (mg/kg)	Pb (mg/kg)	Reference
Bargo River	4.60	0.40	33.7±7.9	36.7±9.9	0.2±0.05	0.08± 0.008	0.1±0.02	1.8±0.02	0.06±0.001	0.2±0.08	This work
Bargo River			3000	5800	< 4	4	3	20		5	Fleming et al. (2021)
Coxs River			5800	30000	16	8	13	43		6	Fleming et al. (2021)
Wollangambe River			270	900	< 4	< 1	< 1	1		< 1	Fleming et al. (2021)
Georges River			1100	4000	< 4	2	1	5		2	Fleming et al. (2021)
Redbank Creek			4000	33000	8	16	6	33		11	Fleming et al. (2021)
Nepan River			990	2400	< 4	2	1	4		2	Fleming et al. (2021)
Port Jackson			895±7	7300±142	6	4	3±1	85±7		18	Jahan and Strezov (2018)
Port Botany			930±28	765±248	-	2±1	-	7±3.6		2	Jahan and Strezov (2018)
Port Kembla			1250±212	8000±778	18.5±20	11±3	20±20	235±78		74±66	Jahan and Strezov (2018)
Port Newcastle			1550±778	5300±566	4	4	3	78 ± 3		24	Jahan and Strezov (2018)
Port Yamba			383±78	760±198	0	1	-	3		1	Jahan and Strezov (2018)
Port Eden			2250±354	46000±46669	29±30	31±17	12±4	2345±2057	0.6	165±205	Jahan and Strezov (2018)
DGV					20	80	21	200	1.5	50	(AGI, 2019)

303

304 *3.2. Effects of pH, sediment properties and initial As solution on adsorption kinetics*

305 **Figures 1a** and **1b** depict the time variation of As(III) and As(V) concentrations in sediment with
306 the different pH levels (4, 7, 10) in aqueous media. It has been reported that the adsorption of
307 As(V) in sediments is stronger under acidic condition (pH 3.7-7.0) and weaker under alkaline
308 conditions (pH 8-10), while the effect of pH on As(III) is weaker (Chen et al., 2016; Maji et al.,
309 2007; Mamindy-Pajany et al., 2011). The PFO and PSO models provided a good fit to
310 experimental data, with the correlation coefficient (R^2) of 0.980-0.999 for As(V) and 0.994-0.998
311 for As(III) (**Table 3**). The amounts of As(III) and As(V) adsorbed on sediment estimated by PSO
312 model were higher than those from PFO model regardless of pH levels, except at pH 4 for As(V).
313 It can be shown that As(III) adsorption was favorable in acidic condition, with equilibrium
314 concentrations in sediment at pH 4 (112.4 mg/kg) being higher than at pH 10 (89.0 mg/kg) or
315 without pH adjustment (105.6 mg/kg). However, the highest As(V) concentration on river
316 sediment (168.6 mg/kg) was at neutral pH, which was slightly higher than its concentration at
317 pH 4 and 10 (**Table 3**). The results for As(V) agreed with the statement that As(V) adsorbed on
318 sediment, which was generally stronger under acidic conditions and weaker under alkaline
319 conditions (Chen et al., 2017; Mamindy-Pajany et al., 2011), while the effect of pH on As(III)
320 was less than As(V) due to its incomplete ionized state (Chen et al., 2017). Ma et a. (2015) also
321 reported that the adsorption of As(III) and As(V) on sediment decreased with an increase in pH,
322 with higher adsorption capacity for As(V) than As(III) at pH 5, 7 and 9. Hence, the results from
323 this study agreed well with the other findings reported.

324

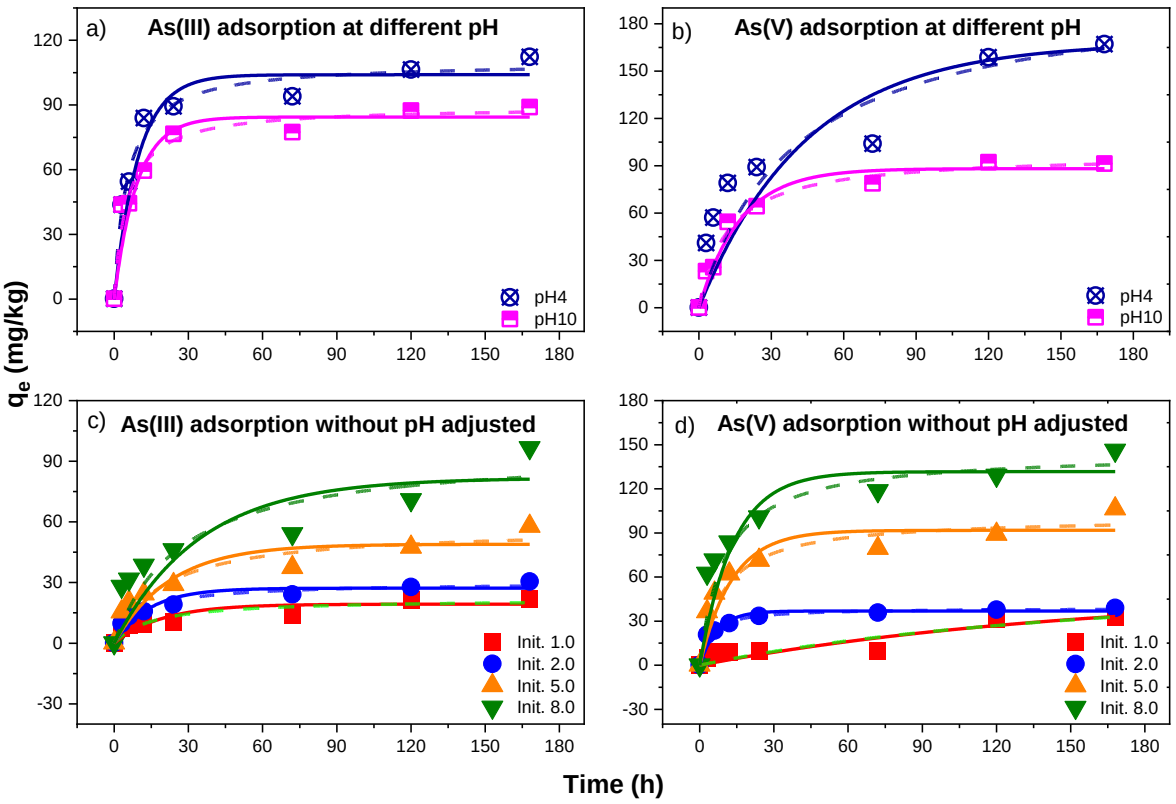

Fig. 1. Effect of pH (a, b) and initial As concentrations in solution (c, d) on the adsorption of As(III) and As(V) on the river sediment. Symbols are experimental data, and the straight and dash lines represent the PFO and PSO kinetic models.

The adsorption of As(III) and As(V) on sediment at varying As concentrations (1-8 mg/L) is shown in **Figs 1c** and **1d**. The rates of As(III) and As(V) adsorption on sediment showed initial rapid stage up to 24 h, followed by a slow stage till the end of experiment. It was suggested that a rapid increase in As adsorption was caused by the enhancement in the SSA with higher reactivity (Xu et al., 2021) and presence of more active surface groups of solid particles, such as COOH and O-H (Rawat et al., 2022). The PFO and PSO fitted well with experimental data, with R^2 values at 0.953-0.999 and 0.989-1.000 for As(III) and As(V), respectively. The estimated q_e values for As(V) at initial concentrations of 1.0 mg/L were 50.0 and 71.1 mg/kg, which were not fitted with the experimental data (32.6 mg/kg). Other estimated results were close to the experimental data (**Table**

340 **3**).

341 The adsorption of As(III) and As(V) on RS and RS-NOM in DI water is shown in **Figs 2 (a**
342 and **b),** while **Fig. 2 (c** and **d)** shows As adsorbed on RS in RW. It can be seen that there was
343 marginal difference between RS and RS-NOM as the adsorbents for As, indicating that NOM had
344 the small effects on As adsorption. Dousova et al. (2012) found that adsorption capacities of
345 As(V) on three sediments increased with an increase in RS and Fe contents. However the
346 adsorption capacity of As(III) only increased with the increase of Fe contents. Xie et al. (2018)
347 pointed out that As(III) and As(V) adsorption on three sediments increased with increasing the
348 RS and clay contents. It is hard to conclude that this study revealed the contradictory results to
349 these outcomes. This comparison may not be completely accurate because the two
350 investigations above used different types of sediment with different characteristics, while only
351 one type of sediment was used in this study. An illustration is that humic acid can bind a portion
352 of As through positively charged amine groups (Varsányi and Kovács, 2006). It is suggested
353 that As adsorption on river sediment is partly prevented because SOM may inhibit the binding
354 of As(III) and As(V) with functional groups of sediment surface. Moreover, the adsorption
355 capacities of both As(III) and As(V) on RS using RW at the equilibrium time were significantly
356 lower than those by using DI water. It was suggested that some element in RS such as anions (PO_4^{3-}
357 , SO_4^{2-}) reduced As species adsorbed on RS.

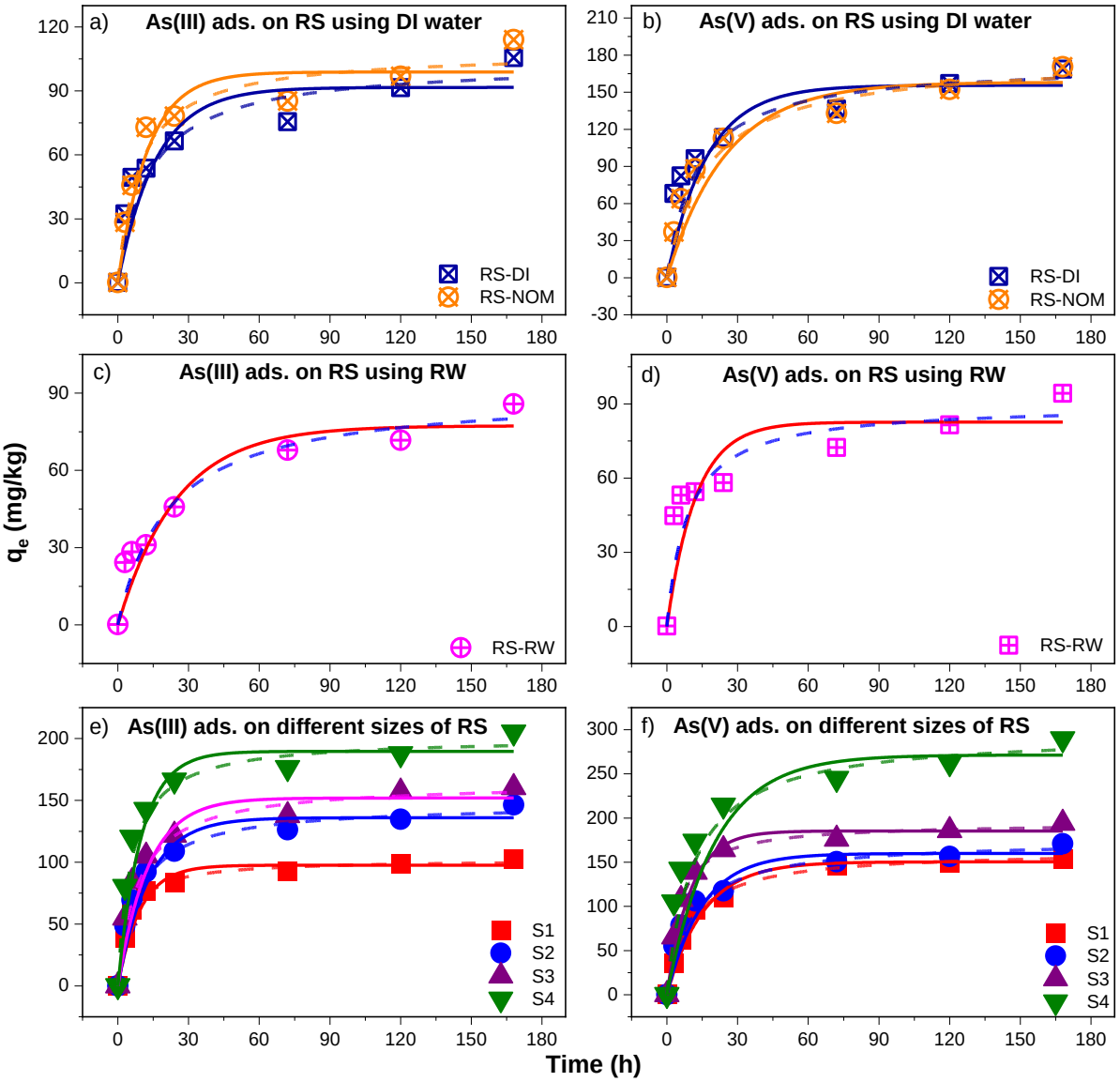

Fig. 2. Adsorption of As(III) and As(V) on RS and RS-NOM (a, b) and sediment fractions (c, d). Symbols are experimental data, and the solid and dash lines represent the PFO and PSO kinetic models.

Figures 3c and **3d** present the PFO and PSO models for adsorption of As(III) and As(V) on different sediment size fractions. The results indicated that a stage of fast adsorption occurred in the first 24h, then the adsorption rate decreased for the rest of experimental duration. Overall, PFO and PSO models provided a good fit to kinetic results with high R^2 values ($\geq$ 0.990) for As(III) and As(V) adsorption (**Table 3**). It can be seen that there was a small difference in As(III) adsorption between S_2 and S_3, while As(V) adsorption on S_1 was close to S_2. Initial As concentrations also had

365 different effects on As(III) and As(V) adsorption. The effect of sediment size on As(III) and
366 As(V) adsorption was significant. **Table 3** shows that the adsorption capacity at equilibrium for
367 As(III) and As(V) increased from 102.2 and 153.2 mg/kg for the largest size (S_1) up to doubled
368 amount for the smallest size (S_4). (**Table 3**). As(V) adsorption capacities on different sediment
369 fractions were higher than those of As(III). Xie et al. (2018) showed similar results with a higher
370 adsorption affinity for A(V) than As(III) related to the smaller sediment sizes. Based on the
371 surface area analysis including RS (4.6 m^2/g), S_1 (3.1 m^2/g), S_2 (6.0 m^2/g), S_3 (6.5 m^2/g) and S_4
372 34.2 m^2/g), S_1 had smaller surface area than RS, resulting in less adsorption capacity, while S_2,
373 S_3 and S_4 showed higher adsorption than RS due to larger surface areas. It is therefore clear that
374 both As(III) and As(V) adsorption on sediment was positively related to the SSA of sediment
375 fractions, but negatively related to the size of sediment fractions. Moreover, finer fractions of
376 RS had better adsorption capacity of As(III) and As(V) due to higher reactivity of these samples.
377 Generally, PSO provided better results in modeling the adsorption kinetics for both As(III)
378 and As(V) than PFO based on the R^2 values. However, Ma et al. (2015) reported better results
379 evaluated by PFO than PSO while the R^2 values were not significantly different between the
380 two models.
381

Table 3. Adsorption kinetics parameters for the PFO and PSO models and equilibrium adsorption capacity.

	Exp. condition	PFO			PSO			Equilibrium
		R^2	K_1 (1/h)	q_e[a] (mg/kg)	R^2	K_2 (kg/mg-h)	q_e[b] (mg/kg)	q_e (mg/kg)
As(III)	pH 4	0.995	0.103	104.0	0.997	0.0017	109.9	112.4
	pH 10	0.997	0.109	84.4	0.998	0.0022	89.4	89.0
	1.0 mg/L	0.998	0.052	19.3	0.998	0.0029	21.9	22.0
	2.0 mg/L	0.999	0.071	27.2	0.999	0.0032	30.0	30.5
	5.0 mg/L	0.992	0.045	49.0	0.995	0.0009	57.1	57.9
	8.0 mg/L	0.975	0.029	81.8	0.983	0.0004	95.6	96.7
	RS-DI	0.987	0.062	91.7	0.992	0.0007	103.5	105.6
	RS-NOM	0.988	0.078	98.9	0.992	0.0010	108.4	114.0
	RS-RW	0.995	0.04	77.3	0.997	0.0006	90.4	85.8
	S_1	0.998	0.106	97.6	0.999	0.0021	102.3	102.2
	S_2	0.995	0.077	136.0	0.998	0.0008	147.2	146.4
	S_3	0.993	0.078	151.9	0.997	0.0007	164.6	160.5
	S_4	0.993	0.102	189.7	0.996	0.0009	200.9	205.2
As(V)	pH 4	0.980	0.023	168.1	0.984	0.0001	203.3	167.1
	pH 10	0.997	0.058	88.2	0.999	0.0008	97.7	91.3
	1.0 mg/L	0.993	0.065	50.0	0.994	0.0001	71.1	32.6
	2.0 mg/L	0.999	0.143	36.9	1.000	0.0067	38.9	39.0
	5.0 mg/L	0.989	0.077	91.8	0.993	0.0010	100.8	106.4
	8.0 mg/L	0.990	0.074	131.7	0.995	0.0007	144.7	146.2
	RS-DI	0.989	0.059	155.6	0.995	0.0005	173.5	168.6
	RS-NOM	0.989	0.040	158.1	0.995	0.0003	178.0	170.6
	RS-RW	0.989	0.08	82.6	0.993	0.0013	89.8	94.3
	S_1	0.999	0.064	105.4	1.000	0.0006	163.4	153.2
	S_2	0.995	0.067	159.9	0.998	0.0005	175.1	170.9
	S_3	0.997	0.101	185.4	0.999	0.0010	194.9	194.2
	S_4	0.990	0.049	271.4	0.996	0.0003	296.3	289.8
Desorption								
As(III)	RS-DI	1.000	0.142	98.6	1.000	0.028	98.1	98.5
As(V)	RS-DI	1.000	0.188	162.4	1.000	0.043	162.0	162.0
As(III)	RS-RW	0.964	0.093	75.9	0.990	0.011	74.9	75.2
As(V)	RS-RW	0.983	0.06	86.3	0.990	0.007	85.1	85.4

Estimated equilibrium adsorption capacity from the PFO model[a] and PSO model[b].

3.3. Kinetic models for desorption process of As(III) and As(V)

Figure 3 displays the desorption kinetics of As(III) and As(V) concentrations in sediment by PFO and PSO models. The results show high-rate desorption at initial stage (0-12 h), followed by stable rate for the remaining duration. The results agree with Ho and McKay (1999) and Ma

et al. (2015) that PFO model can well describe the first stage of sorption kinetics. The amounts of As(III) and As(V) released from RS in RW were less than in DI water, with higher desorbed amounts for As(III) than As(V). The concentrations of As adsorbed on RS at the equilibrium time calculated by PFO and PSO models were close to the experimental data by using both DI water and RW (**Table 3**). Moreover, the PSO model well fitted with all experimental data, indicating that the physicochemical sorption including surface complexation and diffusion to the sorption sites was involved in the desorption processes of both As(III) and As(V). Consequently, the desorption of As(III) and As(V) from this sediment showed similar behavior in terms of kinetics.

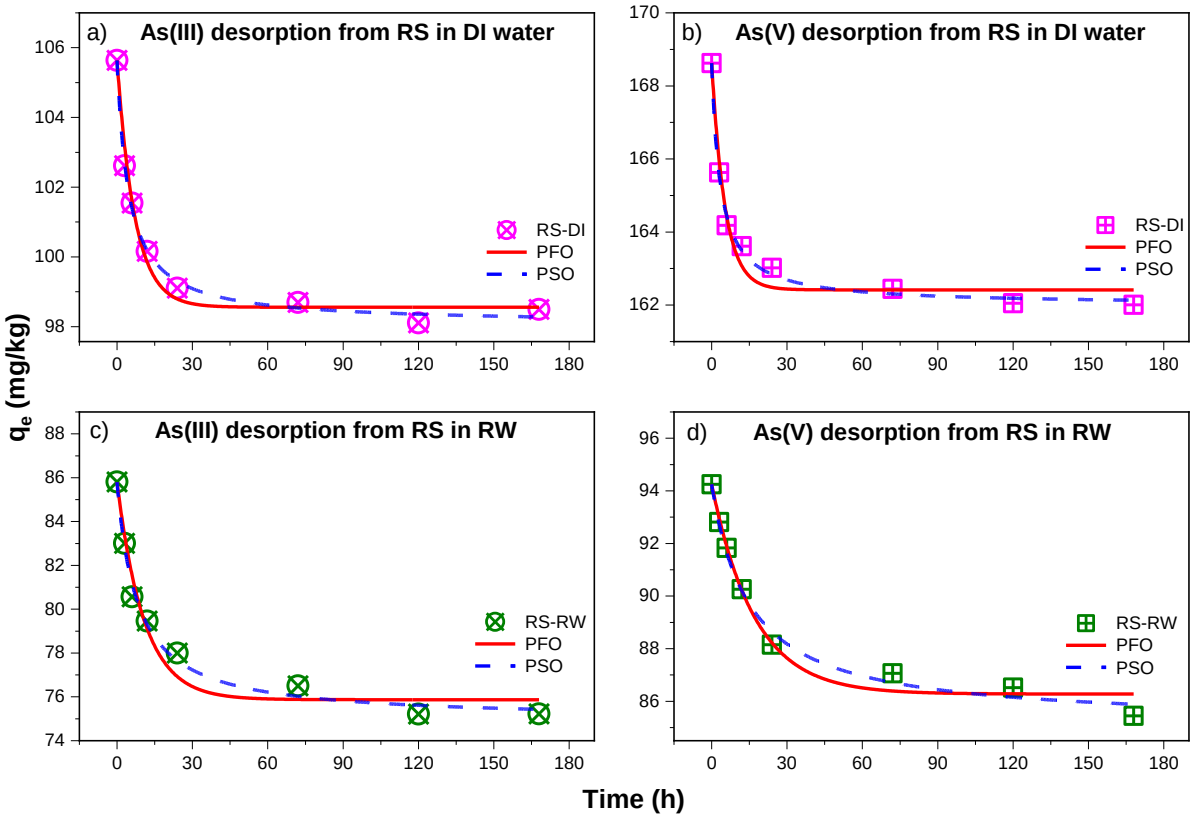

Fig. 3. The nonlinear regression in the PSO and PSO kinetic models of As(III) and As(V) desorption from the RS in DI water (a and b), and RW (c and d).

404 *3.4. Equilibrium adsorption studies*

405 The adsorption isotherms of As(III) and As(V) for RS were modelled by the Langmuir and
406 Freundlich equations (**Figs 4 a, b, c** and **d**). It can be shown that both Langmuir and Freundlich
407 equations fitted well to As(III) and As(V) adsorption isotherms at the equilibrium time with
408 nonlinear behavior. In addition, the best-fit parameter values (q_m, K_L, K_F, n) and R^2 for As(V) and
409 As(III) at the equilibrium time and from the previous studies for sediments are presented in **Table**
410 **4**. In addition, the experimental data in RW was fitted significantly better for both As(III) and
411 As(V) than in DI water, based on the values of reduced chi-squared statistical analysis. The
412 estimated Langmuir maximum adsorption capacity for As(V) was significantly higher than that
413 for As(III) in DI water and lower than in RW. The results in RW were agreement with the findings
414 in Elber River (**Fig. 4e**) from Dousova et al. (2012).
415

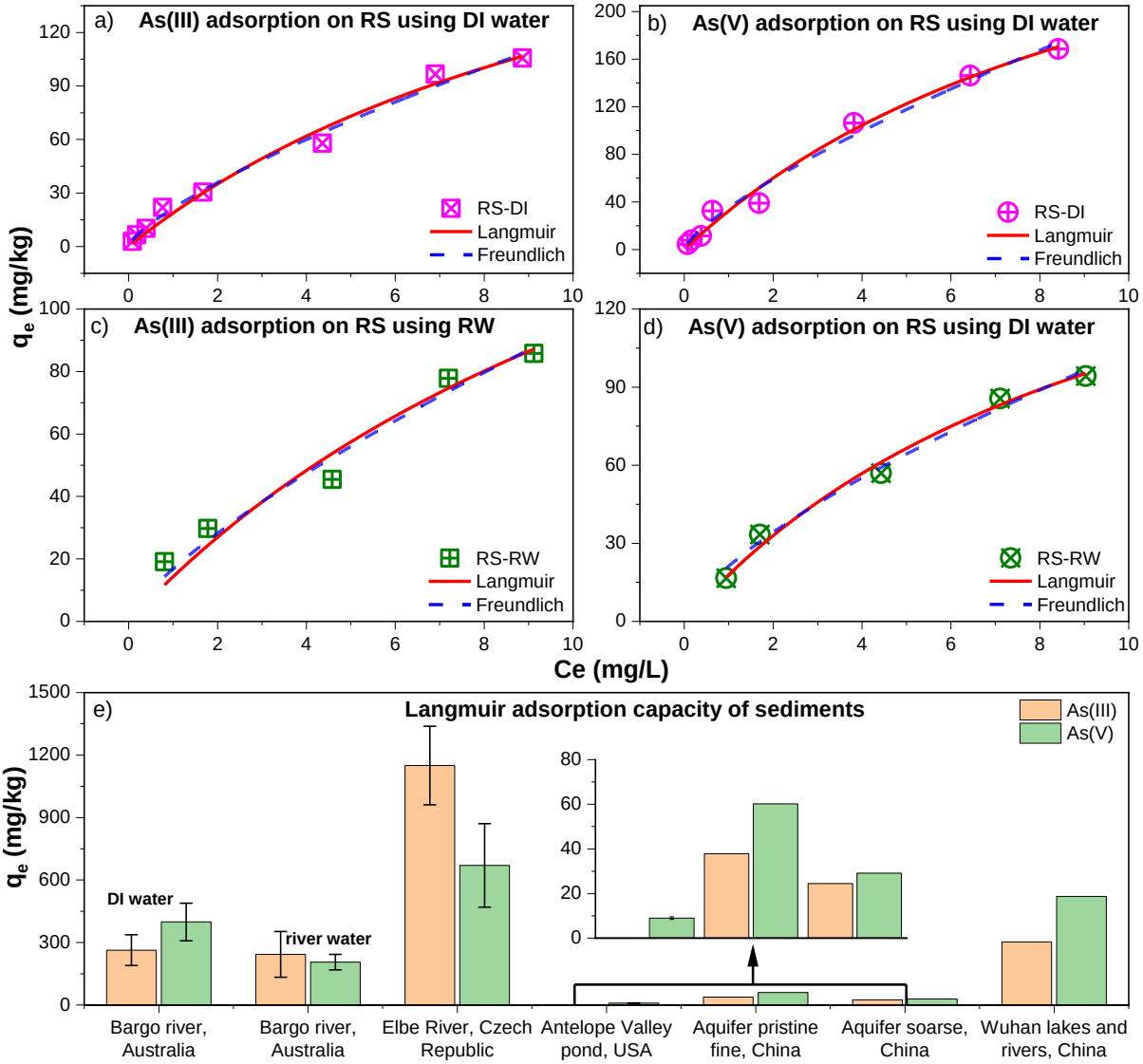

Fig. 4. Adsorption isotherms of (a) As(III) and (b) As(V) on RS in DI water; (c) and (d) in RW; and e) comparison of maximum adsorption amount of As(III) and As(V) on sediment estimated by the Langmuir isotherm model from this work and other studies (Dousova et al., 2012; Goldberg and Suarez, 2013; Ma et al., 2015; Wang et al., 2018).

According to Zhang and Selim (2005), low *1/n* values (< 0.4) indicated extensive heterogeneity of sorption sites. However, the *1/n* values for As(III) and As(V) were 0.74 and 0.75 at the equilibrium time, suggesting some degree of homogeneity of the adsorption sites in the selected sediment. It is suggested that *1/n* values between 0 and 1 are favorable for the adsorption of both As(III) and As(V) on the river sediment. Furthermore, the R_L values for As(III) and As(V)

varied at 0.12-0.92 and 0.098-0.902 at initial As concentrations of 0.11-10.30 mg/L. This indicated favorable adsorption of both As(III) and As(V) on RS, resulting in high surface activity of sediment associated with an increase in As mobility in the sediment-water interface (Dousova et al., 2012). The adsorption maxima (q_m) estimated by the Langmuir equation significantly lower than those of sediments investigated by Dousova et al. (2012) and Wang et al. (2018), and significantly higher than q_m values for As(III) and As(V) adsorbed on sediments from other studies (Goldberg and Suarez, 2013; Ma et al., 2015) (**Fig. 4e**).

In summary, the results calculated by the Langmuir and Freundlich isotherm models in this study showed no significant difference in exhibiting the adsorption mechanism between As(III) and As(V). Ma et al. (2015) reported that Langmuir model can describe homogeneous adsorbent surface while Freundlich model displayed multi-layers of adsorption. Thus, both types of adsorption processes can be fitted well by the data from this study. As a result, As(III) and As(V) adsorption on RS occurs via both chemisorption and physisorption with higher adsorption capacity of As(V) than As(III). These results were in agreement with the findings from Ma et al. (2015) and Wang et al. (2018).

442 **Table 4.** The Langmuir and Freundlich parameters (with standard error) for As(III) and As(V) adsorption from different studies.

	As(III)				As(V)				Reference
Langmuir	q_m (mg/kg)	K_L (L/mg)	Reduced chi-squared	R^2	q_m (mg/kg)	K_L (L/mg)	Reduced chi-squared	R^2	
Bargo river sediment (DI water)	263.3 ±73.8	0.08 ±0.03	27.9	0.986	398.7 ±90.0	0.09 ±0.03	56.5	0.989	This study
Bargo river sediment (RW)	234.3 ±109.9	0.06 ±0.05	0.5	1.000	206.2 ±37.1	0.10 ±0.03	0.1	1.000	This study
SD1, Elbe River	1350	0.0133		0.969	900	0.0133		0.997	Dousova et al. (2012)
SD2, Elbe River	975	0.020		0.972	577.5	0.0124		0.931	Dousova et al. (2012)
SD3, Elbe River	1125	0.0537		0.991	532.5	0.0129		0.964	Dousova et al. (2012)
Surface sediment, Antelope Valley pond					8.96±0.62	0.00082		0.975	Goldberg and Suarez (2013)
Aquifer pristine fine	37.8	0.33		0.990	60.2	0.46		0.974	Ma et al. (2015)
Aquifer coarse[a]	24.5	0.30		0.967	29.1	0.27		0.997	Ma et al. (2015)
Wuhan rivers and lakes[a]	303.3	0.0048		0.936	521.175	0.00268		0.944	Wang et al. (2018)
Freundlich	K_F	n	Reduced chi-squared	R^2	K_F	n	Reduced chi-squared	R^2	
Bargo river sediment (DI water)	21.5 ±2.2	1.35 ±0.10	18.2	0.991	35.1 ±4.2	1.33 ±0.11	68.1	0.987	This study
Bargo river sediment (RW)	16.8 ±1.3	1.34 ±0.19	0.4	1.000	21.2 ±2.9	1.45 ±0.14	0.2	1.000	This study

443

444 *3.4. Sediment-water distribution of As(III) and As(V)*

445 The partition coefficient (K_p) for As(III) and As(V) for both adsorption and desorption is shown
446 in **Fig. 5**. The results were used to provide further understanding of the migration and
447 transformation of As(III) and As(V) between sediments and overlying water. According to
448 Nematollahi et al. (2021), log(K_p) values > 1 reflected a stronger affinity of adsorption and the
449 element strongly remained in the sediment phase compared to lower values. It can be seen that
450 log K_p at pH 4 was higher than that at pH 10, indicating higher adsorption affinity in acidic
451 condition than alkaline solution. **Fig. 5** illustrates the lowest adsorption affinity by using RW
452 for As(III) and at pH 10 for As(V), indicating that the adsorption of As(III) differs from As(V)
453 depending on the environmental conditions. Regarding sediment properties, RS-NOM had
454 marginally higher adsorption affinity than RS for As(III) and the opposite trend was observed
455 for As(V). The effect of sediment sizes was similar for both As species, with the highest
456 adsorption affinity for the smallest size (S_4), then followed by $S_3 > S_2 > S_1$. The log(K_p) values
457 in this study were significantly higher than those investigated from the southern Caspian Sea
458 (mean: 0.35, range: -0.21-0.75) reported by Nematollahi et al. (2021). Moreover, log(K_p) values
459 for As(V) were higher than those of As(III), reflecting higher adsorption affinity of As(V) on
460 sediment than As(III) regardless of controlling factors. The results supported the findings from
461 the early adsorption kinetic and isotherm results.

462 The results showed lower log K_p for As(III) than As(V), indicating that As(III) was more
463 easily released from sediment to water phase in comparison to As(V). The amount of As(III)
464 released from RS (7.2 mg/kg in DI water and 10.6 mg/kg in RW) at the equilibrium of
465 desorption process was higher than for As(V) (6.6 and 8.8 mg/kg, respectively), which is
466 consistent with the K_p results. Overall, these results are consistent with those of Nematollahi et
467 al. (2021).

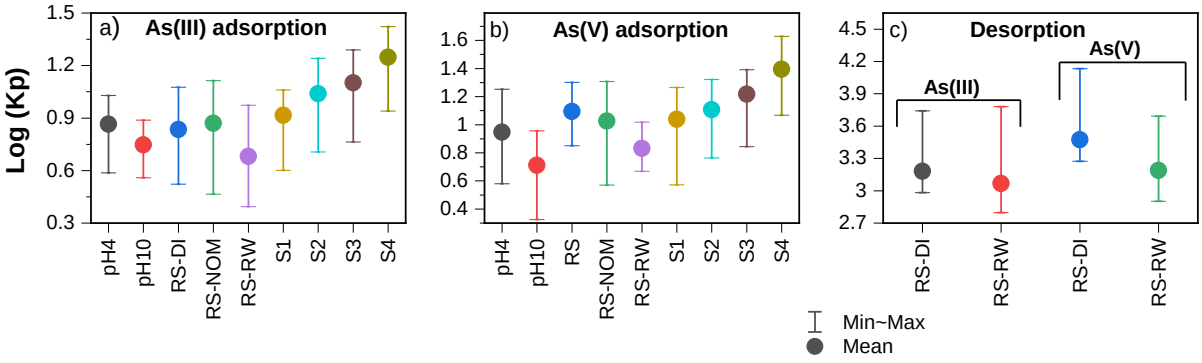

Fig. 5. Partition coefficient of As(III) and As(V) under different conditions.

468

469 *3.5. As adsorption mechanisms*

470 As(III) and As(V) forms present in aqueous media described in the **Fig. 6** (Mondal et al., 2007;

471 Yin et al., 2019; Yohai et al., 2019).

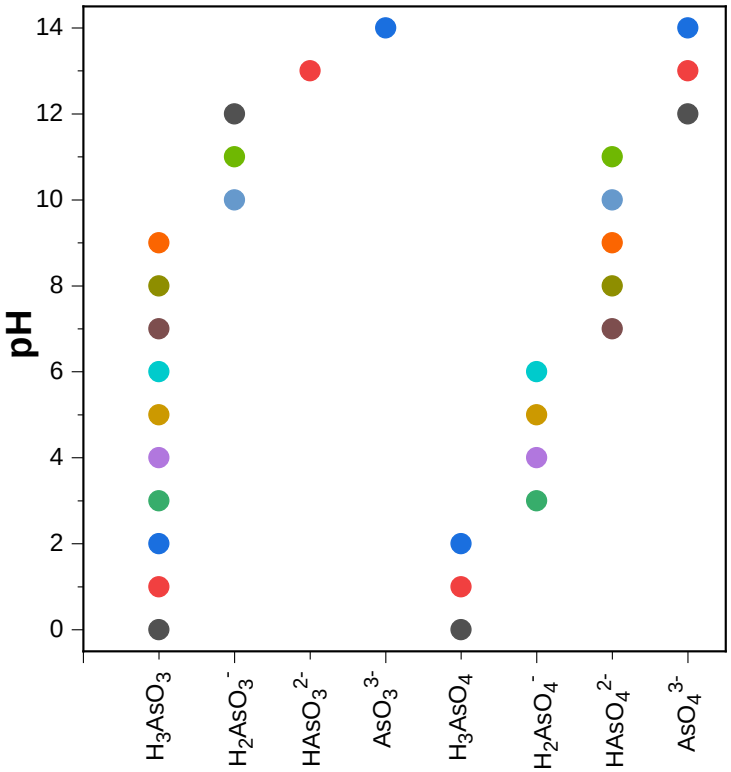

472

473 **Fig. 6.** The forms of As(III) and As(V) in the aqueous media

474

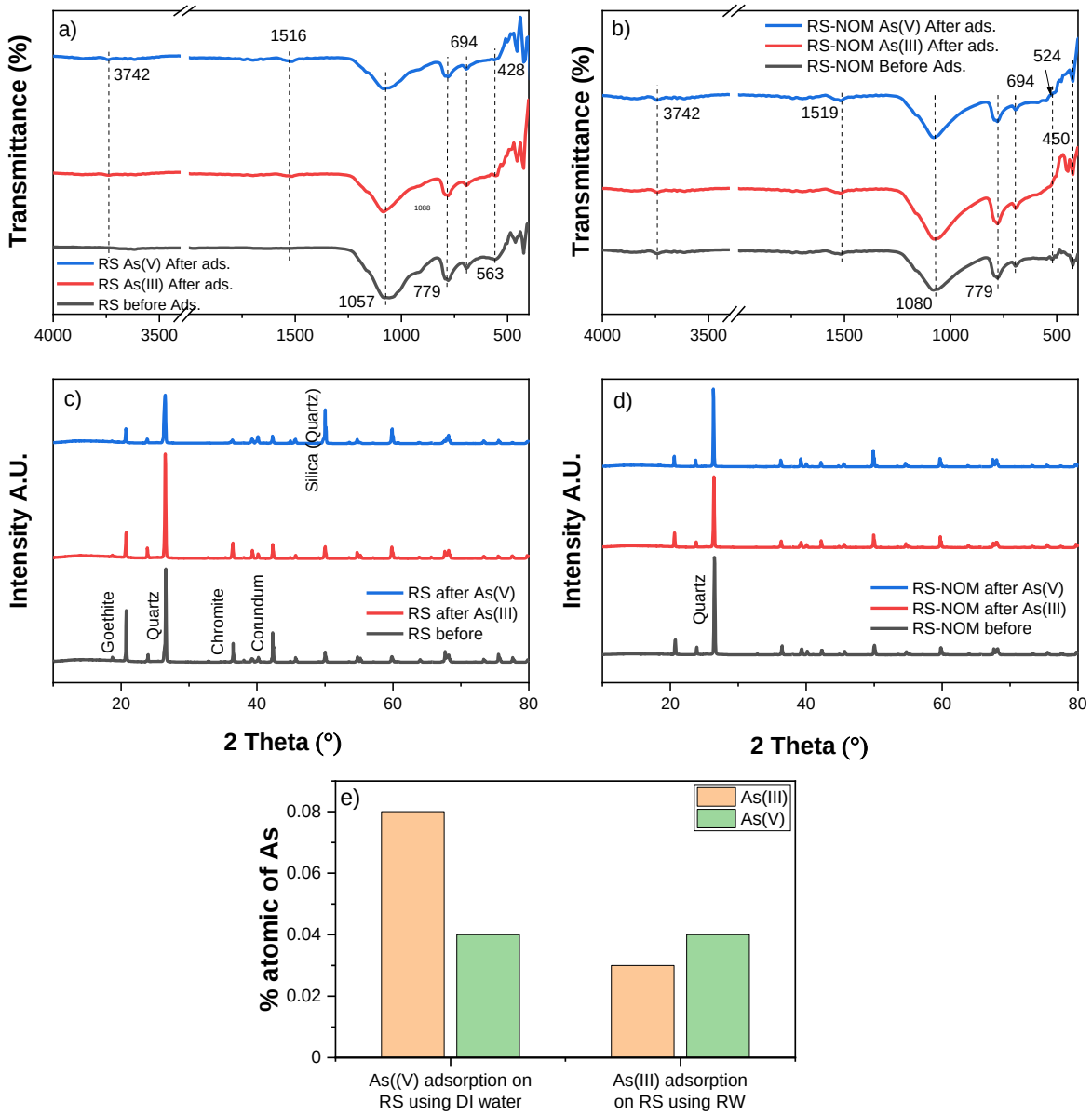

Fig. 7. FTIR spectra (400-4000 cm^{-1}) of (a) RS and (b) RS-NOM; XRD patterns of (c) RS and (d) and RS-NOM before and after adsorption of As(III) and As(V); (e) As transformation between As(III) and As(V) on RS after adsorption

The interaction between As(III) and As(V) and with sediment particles in the adsorption process was investigated by performing FTIR of different sediment types including RS and RS-NOM before and after As(III) and As(V) adsorption. The FTIR spectra for SOM are shown in **Fig. 7a**. A new IR adsorption peak appeared at 1516 cm^{-1} after the adsorption of As(III) and As(V) on SOM, which can be attributed to carboxyl groups (Kaufhold et al., 2012; Li et al., 2018) or amine C=O stretching (Yu et al., 2015). The band at 3742 cm^{-1} corresponds to O–H

stretching vibrations of phenolic hydroxyl groups or adsorbed water (Luo et al., 2012; Yu et al., 2015). The IR peaks shifted from 1057 cm^{-1} to 1088 cm^{-1} and 1080 cm^{-1} after adsorption of As(III) and As(V), which can be associated with Si(Al)–O vibration or antisymmetric stretching vibrations of Si–O tetrahedron (Hahn et al., 2018). The IR adsorption bands recorded at 779 cm^{-1} before adsorption and 787 cm^{-1} as well as 694 cm^{-1} for all samples are assigned to Si–O symmetrical stretching vibrations of quartz, exhibiting the roles of these surface functional moieties in As(III) and As(V) binding with sediment particles (Hahn et al., 2018; Rawat et al., 2022). Furthermore, the small shift in the IR peaks from 563 cm^{-1} to 553 cm^{-1} and 559 cm^{-1} after adsorption of As(III) and As(V), respectively can be contributed to the involvement of Fe–O/Fe–OH vibration of the magnetite phase in the As(III) and As(V) adsorption (Luo et al., 2012; Rawat et al., 2022). Finally, the IR bands at around 420-428 cm^{-1} before and after As(V) adsorption can be related to the formation of Si–O–Mn bonds (Hahn et al., 2018; Kaufhold et al., 2012), while its disappearance after As(III) adsorption indicated the involvement of these functional groups in As(III) binding with sediment particles.

Furthermore, the SEM-EDS images of RS before and after adsorption of As(III) and As(V) are given in **Fig. S2**. **Fig. S2 (a, b** and **d)** showed high Al contents were detected on RS before and after adsorption of As(III), while **Fig. S2 (c** and **e)** showed low Al contents were found on RS after adsorption of As(V). The results indicated higher enrichment of As(V) on RS than As(III) (Matera et al., 2003). Moreover, XPS results showed no detection of As for RS before and after adsorption of As(III) by using DI water and As(V) by RW solution, whilst both As2p3A and As2p3B corresponding to As(III) and As(V) were detected on RS after adsorption of As(V) under DI water and As(III) under RW (**Fig. S3**). The results indicate that there was oxidation from As(III) to As(V) in DI water and reduction from As(V) to As(III) in RW after adsorption on RS (Guo et al., 2022). Additionally, Fig. 6e indicated the transformation between these As species in RS after adsorption with higher amount of As(V) reduced to As(III) than oxidation process. **Fig. S3(a, b** and **e)** showed no detection of As on RS due to low content of

As in sediment (before adsorption).

Regarding RS-NOM, no new groups appeared in the FTIR diagram (**Fig. 7b**), indicating that the interaction between As(III) and As(V) and sediment particles only occurred in the available functional groups of sediments. Moreover, the IR bands under 500 cm^{-1} can be assigned to Si–O–Mn bonds (Hahn et al., 2018; Kaufhold et al., 2012), which disappeared after adsorption of As(III) on RS and indicated the involvement of these functional groups in As(III) binding with sediment particles. XRD analysis for RS and RS-NOM before and after adsorption of As(III) and As(V) (**Figs 7c** and **d**) indicated that quartz was dominant and had the strongest peak in all samples. The results are similar to findings from previous studies of XRD for river sediments (Maity and Maiti, 2016; Xie et al., 2018). Hahn et al. (2018) indicated that quartz peaks corresponding to the Si-O-Si symmetric stretching of antisymmetric stretching vibrations. Additionally, the changes of quartz peaks may be due to either reaction of anionic As species with organic-Si or with SiO_2 in the presence of organic matter (Rawat et al., 2022).

4. Conclusions

The adsorption and desorption of As(III) and As(V) at sediment-water interface were studied. Adsorption kinetics were well modeled by both PFO and PSO models, with better results by PSO based on the R^2 values. The Langmuir and Freundlich equations well modeled As(III) and As(V) adsorption equilibrium on sediment. The maximum adsorption capacity of As(V) (398.7 mg/kg) was higher than that of As (III) (263.3 mg/kg), indicating stronger sediment affinity toward As(V) than As(III). The results also showed that As(III) and As(V) adsorption on river sediment was favored at acidic to neutral conditions. SOM caused a reduction of As(III) and As(V) adsorption on sediment, by inhibiting As complexation with sediment functional groups. As adsorption decreased with increasing sediment particle size, and increased with sediment surface area. The physicochemical characteristics, FTIR and XRD analysis of sediment showed that As(III) and As(V) adsorption on sediment occurred by

interactions with Fe–O/Fe–OH, Si(Al)–O, hydroxyl and carboxyl functional groups. The SEM-EDS evidenced higher adsorption of As(V) than As(III) and there was transformation among As species during the adsorption process in both DI water and RW. The results provide valuable insights on the kinetics, equilibrium, and mechanism of As(III)/As(V) adsorption on river sediment, which should be considered for the more effective management of As-contaminated river sediments.

Declaration of Competing Interest

The authors declare no conflict of interest.

References

AGI, 2019. Toxicant default guideline values for sediment quality. Australian Government Initiative. https://www.waterquality.gov.au/anz-guidelines/guideline-values/default/sediment-quality-toxicants.

Akter, K.F., Owens, G., Davey, D.E., Naidu, R., 2006. Arsenic speciation and toxicity in biological systems. Rev. Environ. Contam. Toxicol. 184. https://doi.org/10.1007/0-387-27565-7_3

Ali, A. e., Strezov, V., Davies, P.J., Wright, I., 2018. River sediment quality assessment using sediment quality indices for the Sydney basin, Australia affected by coal and coal seam gas mining. Sci. Total Environ. 616–617, 695–702. https://doi.org/10.1016/J.SCITOTENV.2017.10.259

Alkurdi, S.S.A., Al-Juboori, R.A., Bundschuh, J., Bowtell, L., Marchuk, A., 2021. Inorganic arsenic species removal from water using bone char: A detailed study on adsorption kinetic and isotherm models using error functions analysis. J. Hazard. Mater. 405, 124112. https://doi.org/10.1016/J.JHAZMAT.2020.124112

Arco-Lázaro, E., Agudo, I., Clemente, R., Bernal, M.P., 2016. Arsenic(V) adsorption-

559 desorption in agricultural and mine soils: Effects of organic matter addition and phosphate
560 competition. Environ. Pollut. 216, 71–79. https://doi.org/10.1016/j.envpol.2016.05.054
561 Azizian, S., 2004. Kinetic models of sorption: a theoretical analysis. J. Colloid Interface Sci.
562 276, 47–52. https://doi.org/10.1016/J.JCIS.2004.03.048
563 Chen, X., Sun, Q., Ding, S., Chen, M., Fan, X., Zhang, L., Zhang, C., 2017. Mobile Arsenic
564 Distribution and Release Kinetics in Sediment Profiles under Varying pH Conditions.
565 Water. Air. Soil Pollut. 228, 1–12. https://doi.org/10.1007/s11270-017-3601-4
566 De Jonge, M., Teuchies, J., Meire, P., Blust, R., Bervoets, L., 2012. The impact of increased
567 oxygen conditions on metal-contaminated sediments part I: Effects on redox status,
568 sediment geochemistry and metal bioavailability. Water Res. 46, 2205–2214.
569 https://doi.org/10.1016/J.WATRES.2012.01.052
570 Dias, F.F., Allen, H.E., Guimarães, J.R., Taddei, M.H.T., Nascimento, M.R., Guilherme,
571 L.R.G., 2009. Environmental behavior of arsenic(III) and (V) in soils. J. Environ. Monit.
572 11, 1412–1420. https://doi.org/10.1039/b900545e
573 Dong, Y., Gao, M., Song, Z., Qiu, W., 2020. As(III) adsorption onto different-sized polystyrene
574 microplastic particles and its mechanism. Chemosphere 239.
575 https://doi.org/10.1016/j.chemosphere.2019.124792
576 Dong, Y., Gao, M., Song, Z., Qiu, W., 2019. Adsorption mechanism of As(III) on
577 polytetrafluoroethylene particles of different size. Environ. Pollut. 254, 112950.
578 https://doi.org/10.1016/J.ENVPOL.2019.07.118
579 Dousova, B., Buzek, F., Rothwell, J., Krejcova, S., Lhotka, M., 2012. Adsorption behavior of
580 arsenic relating to different natural solids: Soils, stream sediments and peats. Sci. Total
581 Environ. 433, 456–461. https://doi.org/10.1016/J.SCITOTENV.2012.06.063
582 Ellwood, M.J., Maher, W.A., 2003. Measurement of arsenic species in marine sediments by
583 high-performance liquid chromatography–inductively coupled plasma mass spectrometry.
584 Anal. Chim. Acta 477, 279–291. https://doi.org/10.1016/S0003-2670(02)01414-9

585 Fang, Z., Wang, Y., Xie, D., Wang, D., 2021. Potential Ecological Risk of Heavy Metals in a
586 Typical Tributary of the Three Gorges Reservoir. Bull. Environ. Contam. Toxicol. 106.
587 https://doi.org/10.1007/s00128-020-03014-5
588 Feng, Q., Zhang, Zhiyong, Chen, Y., Liu, L., Zhang, Zhengjie, Chen, C., 2013. Adsorption and
589 Desorption Characteristics of Arsenic on Soils: Kinetics, Equilibrium, and Effect of
590 Fe(OH)3 Colloid, H2SiO3 Colloid and Phosphate. Procedia Environ. Sci. 18, 26–36.
591 https://doi.org/https://doi.org/10.1016/j.proenv.2013.04.005
592 Fleming, C., Morrison, K., Robba, L., Reynolds, J., Wright, I.A., 2021. 14-Month Water
593 Quality Investigation of Coal Mine Discharge on Two Rivers in NSW, Australia:
594 Implications for Environmental Regulation. Water. Air. Soil Pollut. 232.
595 https://doi.org/10.1007/s11270-021-05020-7
596 Foo, K.Y., Hameed, B.H., 2010. Insights into the modeling of adsorption isotherm systems.
597 Chem. Eng. J. 156, 2–10. https://doi.org/10.1016/j.cej.2009.09.013
598 Garneau, C., Sauvage, S., Probst, A., Sánchez-Pérez, J.M., 2015. Modelling of trace metal
599 transfer in a large river under different hydrological conditions (the Garonne River in
600 southwest France). Ecol. Modell. 306, 195–204.
601 https://doi.org/10.1016/j.ecolmodel.2014.09.011
602 Gedik, K., Kongchum, M., Boran, M., Delaune, R.D., 2016. Adsorption and desorption of
603 arsenate in Louisiana rice soils. Arch. Agron. Soil Sci. 0340, 856–864.
604 https://doi.org/10.1080/03650340.2015.1096015
605 Goldberg, S., Suarez, D.L., 2013. Arsenate Adsorption by Unsaturated Alluvial Sediments. Soil
606 Sci. Soc. Am. J. 77, 782–791. https://doi.org/10.2136/sssaj2012.0322
607 Grafe, M., Eick, M.J., Grossl, P.R., 2001. Adsorption of Arsenate (V) and Arsenite (III) on
608 Goethite in the Presence and Absence of Dissolved Organic Carbon; Adsorption of
609 Arsenate (V) and Arsenite (III) on Goethite in the Presence and Absence of Dissolved
610 Organic Carbon, Soil Sci. Soc. Am. J. 65, 1680-1687.

611 Guo, H., Stüben, D., Berner, Z., 2007. Adsorption of arsenic(III) and arsenic(V) from
612 groundwater using natural siderite as the adsorbent. J. Colloid Interface Sci. 315, 47–53.
613 https://doi.org/10.1016/j.jcis.2007.06.035
614 Hahn, A., Vogel, H., Andó, S., Garzanti, E., Kuhn, G., Lantzsch, H., Schüürman, J., Vogt, C.,
615 Zabel, M., 2018. Using Fourier transform infrared spectroscopy to determine mineral
616 phases in sediments. Sediment. Geol. 375, 27–35.
617 https://doi.org/10.1016/J.SEDGEO.2018.03.010
618 Hettiarachchi, S.R., Maher, W.A., Krikowa, F., Ubrihien, R., 2017. Factors influencing arsenic
619 concentrations and species in mangrove surface sediments from south-east NSW,
620 Australia. Environ. Geochem. Health 39, 209–219. https://doi.org/10.1007/s10653-016-
621 9821-5
622 Ho, Y.S., McKay, G., 1999. Pseudo-second order model for sorption processes. Process
623 Biochem. 34, 451–465. https://doi.org/10.1016/S0032-9592(98)00112-5
624 Hoogsteen, M.J.J., Lantinga, E.A., Bakker, E.J., Tittonell, P.A., 2018. Communications in Soil
625 Science and Plant Analysis An Evaluation of the Loss-on-Ignition Method for
626 Determining the Soil Organic Matter Content of Calcareous Soils An Evaluation of the
627 Loss-on-Ignition Method for Determining the Soil Organic Matter Content. Commun. Soil
628 Sci. Plant Anal. 49, 1541–1552. https://doi.org/10.1080/00103624.2018.1474475
629 Huang, G., Chen, Z., Wang, J., Sun, J., Liu, J., Zhang, Y., 2013. Adsorption of arsenite onto a
630 soil irrigated by sewage. J. Geochemical Explor. 132, 164–172.
631 https://doi.org/10.1016/j.gexplo.2013.06.015
632 Jahan, S., Strezov, V., 2018. Comparison of pollution indices for the assessment of heavy
633 metals in the sediments of seaports of NSW, Australia. Mar. Pollut. Bull. 128, 295–306.
634 https://doi.org/10.1016/j.marpolbul.2018.01.036
635 Kaufhold, S., Hein, M., Dohrmann, R., Ufer, K., 2012. Quantification of the mineralogical
636 composition of clays using FTIR spectroscopy. Vib. Spectrosc. 59, 29–39.

637 https://doi.org/10.1016/J.VIBSPEC.2011.12.012
638 Kumar, R.R., Kumar, R.R., Mittal, S., Arora, M., Babu, J.N., 2016. Role of soil
639 physicochemical characteristics on the present state of arsenic and its adsorption in alluvial
640 soils of two agri-intensive region of Bathinda, Punjab, India. J. Soils Sediments 16, 605–
641 620. https://doi.org/10.1007/s11368-015-1262-8
642 Kundu, S., Gupta, A.K., 2006. Arsenic adsorption onto iron oxide-coated cement (IOCC):
643 Regression analysis of equilibrium data with several isotherm models and their
644 optimization. Chem. Eng. J. 122, 93–106. https://doi.org/10.1016/j.cej.2006.06.002
645 Li, H., Wang, J., Zhao, B., Gao, M., Shi, W., Zhou, H., Xie, Z., Zhou, B., Lü, C., He, J., 2018.
646 The role of major functional groups: Multi-evidence from the binding experiments of
647 heavy metals on natural fulvic acids extracted from lake sediments. Ecotoxicol. Environ.
648 Saf. 162, 514–520. https://doi.org/10.1016/J.ECOENV.2018.07.038
649 Luo, T., Sun, J., Liu, Y., Cui, L., Fu, Q., 2019. Adsorption and transport behavior of arsenate
650 on saline-alkali soils of tidal flat of Yellow Sea, Eastern China. Environ. Pollut.
651 Bioavailab. 31, 166–173. https://doi.org/10.1080/26395940.2019.1604162
652 Luo, X., Wang, C., Luo, S., Dong, R., Tu, X., Zeng, G., 2012. Adsorption of As (III) and As
653 (V) from water using magnetite Fe3O4-reduced graphite oxide–MnO2 nanocomposites.
654 Chem. Eng. J. 187, 45–52. https://doi.org/10.1016/J.CEJ.2012.01.073
655 Ma, J., Guo, H., Lei, M., Zhou, X., Li, F., Yu, T., Wei, R., Zhang, H., Zhang, X., Wu, Y., 2015.
656 Arsenic Adsorption and its Fractions on Aquifer Sediment: Effect of pH, Arsenic Species,
657 and Iron/Manganese Minerals. Water Air Soil Pollut. 226, 260.
658 https://doi.org/10.1007/s11270-015-2524-1
659 Maity, S.K., Maiti, R., 2016. Understanding the sediment sources from mineral composition at
660 the lower reach of Rupnarayan River, West Bengal, India – XRD-based analysis. GeoResJ
661 9–12. https://doi.org/10.1016/j.grj.2016.09.004
662 Mamindy-Pajany, Y., Hurel, C., Marmier, N., Roméo, M., 2011. Arsenic (V) adsorption from

aqueous solution onto goethite, hematite, magnetite and zero-valent iron: Effects of pH, concentration and reversibility. Desalination 281, 93–99. https://doi.org/10.1016/j.desal.2011.07.046

Mondal, P., Balomajumder, C., Mohanty, B., 2007. A laboratory study for the treatment of arsenic, iron, and manganese bearing ground water using Fe3+ impregnated activated carbon: Effects of shaking time, pH and temperature. J. Hazard. Mater. 144, 420–426. https://doi.org/10.1016/j.jhazmat.2006.10.078

Nematollahi, M.J., Keshavarzi, B., Moore, F., Vogt, R.D., Nasrollahzadeh Saravi, H., 2021. Trace elements in the shoreline and seabed sediments of the southern Caspian Sea: investigation of contamination level, distribution, ecological and human health risks, and elemental partition coefficient. Environ. Sci. Pollut. Res. https://doi.org/10.1007/s11356-021-14678-9

Nguyen, K.T., Ahmed, M.B., Mojiri, A., Huang, Y., Zhou, J.L., Li, D., 2021. Advances in As contamination and adsorption in soil for effective management. J. Environ. Manage. 296, 113274. https://doi.org/10.1016/j.jenvman.2021.113274

Plant, J., Kinniburg, D., Smedley, Fordyce, F., Klinck, B., 2005. Arsenic and Selenium, in: British Geological Survey.

Rawat, A.P., Kumar, V., Singh, P., Shukla, A.C., Singh, D.P., 2022. Kinetic Behavior and Mechanism of Arsenate Adsorption by Loam and Sandy Loam Soil Kinetic Behavior and Mechanism of Arsenate Adsorption by Loam and Sandy Loam Soil. Soil Sediment Contam. An Int. J. 31, 15-39. https://doi.org/10.1080/15320383.2021.1900071

Smith, E., Smith, J., Naidu, R., 2006. Distribution and nature of arsenic along former railway corridors of South Australia. Sci. Total Environ. 363, 175–182. https://doi.org/10.1016/j.scitotenv.2005.05.039

Tang, L., Feng, H., Tang, J., Zeng, G., Deng, Y., Wang, J., Liu, Y., Zhou, Y., 2017. Treatment of arsenic in acid wastewater and river sediment by Fe@Fe2O3 nanobunches: The effect

689 of environmental conditions and reaction mechanism. Water Res. 117, 175–186.
690 https://doi.org/10.1016/j.watres.2017.03.059
691 Tseng, J.Y., Chang, C.Y., Chang, C.F., Chen, Y.H., Chang, C.C., Ji, D.R., Chiu, C.Y., Chiang,
692 P.C., 2009. Kinetics and equilibrium of desorption removal of copper from magnetic
693 polymer adsorbent. J. Hazard. Mater. 171. https://doi.org/10.1016/j.jhazmat.2009.06.030
694 Varsányi, I., Kovács, L.Ó., 2006. Arsenic, iron and organic matter in sediments and
695 groundwater in the Pannonian Basin, Hungary. Appl. Geochemistry 21, 949–963.
696 https://doi.org/10.1016/j.apgeochem.2006.03.006
697 Wang, J., Xu, J., Xia, J., Wu, F., Zhang, Y., 2018. A kinetic study of concurrent arsenic
698 adsorption and phosphorus release during sediment resuspension. Chem. Geol. 495, 67–
699 75. https://doi.org/https://doi.org/10.1016/j.chemgeo.2018.08.003
700 Xie, Y., Lu, G., Yang, C., Qu, L., Chen, M., Guo, C., Dang, Z., 2018. Mineralogical
701 characteristics of sediments and heavy metal mobilization along a river watershed affected
702 by acid mine drainage. PLoS One 13, 1–17. https://doi.org/10.1371/journal.pone.0190010
703 Xie, Z., Wang, Jia, Wei, X., Li, F., Chen, M., Wang, Jing, Gao, B., 2018. Interactions between
704 arsenic adsorption/desorption and indigenous bacterial activity in shallow high arsenic
705 aquifer sediments from the Jianghan Plain, Central China. Sci. Total Environ. 644, 382–
706 388. https://doi.org/https://doi.org/10.1016/j.scitotenv.2018.06.377
707 Yin, Z., Lützenkirchen, J., Finck, N., Celaries, N., Dardenne, K., Hansen, H.C.B., 2019.
708 Adsorption of arsenic(V) onto single sheet iron oxide: X-ray absorption fine structure and
709 surface complexation. J. Colloid Interface Sci. 554, 433–443.
710 https://doi.org/10.1016/J.JCIS.2019.07.024
711 Yohai, L., Giraldo, H., Mejía, M., Procaccini, R., Pellice, S., Laxman Kunjali, K., Dutta, J.,
712 Uheida, A., 2019. Nanocomposite functionalized membranes based on silica nanoparticles
713 cross-linked to electrospun nanofibrous support for arsenic(V) adsorption from
714 contaminated underground water †. RSC Adv. 9, 8280–8289.

https://doi.org/10.1039/c8ra09866b

Yu, Z., Zhou, L., Huang, Y., Song, Z., Qiu, W., 2015. Effects of a manganese oxide-modified biochar composite on adsorption of arsenic in red soil. J. Environ. Manage. 163, 155–162. https://doi.org/10.1016/J.JENVMAN.2015.08.020

Zhang, H., Selim, H.M., 2005. Kinetics of arsenate adsorption - desorption in soils. Environ. Sci. Technol. 39, 6101–6108. https://doi.org/10.1021/es050334u

Guo, J., Yin, Z., Zhong, W., Jing, C., 2022. Immobilization and transformation of co-existing arsenic and antimony in highly contaminated sediment by nano zero-valent iron. Journal of Environmental Sciences, 112, 152-160.

Maji, S. K., Pal, A., Pal, T., Adak, A., 2007. Modeling and fixed bed column adsorption of As(III) on laterite soil. Separation and Purification Technology, 56(3), 284-290.

Matera, V., Le Hécho, I., Laboudigue, A., Thomas, P., Tellier, S., Astruc, M., 2003. A methodological approach for the identification of arsenic bearing phases in polluted soils. Environmental Pollution, 126(1), 51-64.

SIMEC, 2021, September 30. Monthly Water Record. SIMEC. http://www.simec.com/media/7195/monthly-water_sept-2021.pdf.

Wang, S., Mulligan, C.N., 2006. Natural attenuation processes for remediation of arsenic contaminated soils and groundwater. Journal of Hazardous Materials, 138(3), 459-470.

Xu, J., Bland, G.D., Gu, Y., Ziaei, H., Xiao, X., Deonarine, A., Reible, D., Bireta, P., Hoelen, T.P., Lowry, G.V., 2021. Impacts of Sediment Particle Grain Size and Mercury Speciation on Mercury Bioavailability Potential. Environmental Science and Technology, 55(18), 12393-12402.